JACS
JOURNAL OF THE AMERICAN CHEMICAL SOCIETY
pubs.acs.org/JACS
Article

Hydrogen Storage with Aluminum Formate, ALF: Experimental, Computational, and Technoeconomic Studies

Hayden A. Evans,* Taner Yildirim,* Peng Peng, Yongqiang Cheng, Zeyu Deng, Qiang Zhang, Dinesh Mullangi, Dan Zhao, Pieremanuele Canepa, Hanna M. Breunig, Anthony K. Cheetham, and Craig M. Brown*

Cite This: https://doi.org/10.1021/jacs.3c08037

ABSTRACT: Long-duration storage of hydrogen is necessary for coupling renewable H_2 with stationary fuel cell power applications. In this work, aluminum formate (ALF), which adopts the ReO_3-type structure, is shown to have remarkable H_2 storage performance at non-cryogenic (>120 K) temperatures and low pressures. The most promising performance of ALF is found between 120 K and 160 K and at 10 bar to 20 bar. The study illustrates H_2 adsorption performance of ALF over the 77 K to 296 K temperature range using gas isotherms, in situ neutron powder diffraction, and DFT calculations, as well as technoeconomic analysis (TEA), illustrating ALF's competitive performance for long-duration storage versus compressed hydrogen and leading metal−organic frameworks. In the TEA, it is shown that ALF's storage capacity, when combined with a temperature/pressure swing process, has advantages versus compressed H_2 at a fraction of the pressure (15 bar versus 350 bar). Given ALF's performance in the 10 bar to 20 bar regime under moderate cooling, it is particularly promising for use in safe storage systems serving fuel cells.

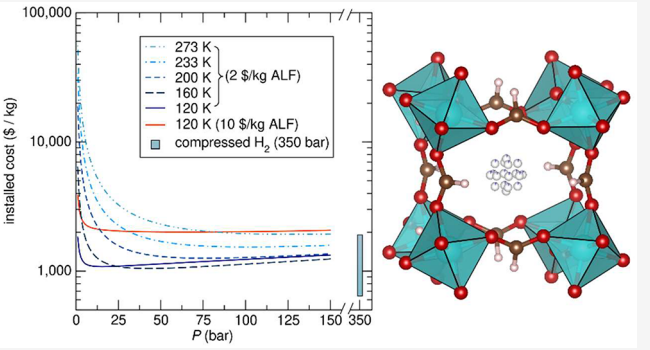

INTRODUCTION

Stationary hydrogen-powered fuel cells are emerging as a solution for delivering clean and flexible power.[1−3] Renewable-energy-powered electrolysis can generate hydrogen but may require multiple days' worth of hydrogen storage to smooth renewable-energy variability. Storage is also needed in cases where hydrogen is used as a backup power system, with a necessary target storage duration of 96 h to meet the requirements set by the United States National Fire Protection Association. This presents a challenge, as compressed gas or cryogenic hydrogen storage is operationally expensive and inefficient at large scales for these storage durations, and salt caverns proposed for storage are not widely available and require pipelines to make them suitable for significantly larger applications. As such, much work has been conducted to identify material-based solutions for hydrogen storage that operate at lower pressures and warmer temperatures.[4]

A recent analysis by some of the authors of stationary hydrogen storage for long-duration energy supply suggests there is potential for porous metal−organic frameworks (MOFs) to perform well in such applications.[5] These materials can adsorb H_2 within their porous structures and via gas−framework interactions, facilitating high hydrogen storage capacities. However, a MOF's peak adsorption under equilibrium conditions is only one indicator of promise, and a MOF must be holistically evaluated across other key factors, such as the constraints resulting from integration with electrolyzer and fuel cell systems. Fuel cells require high-purity hydrogen at fast delivery rates and modest pressures, which MOFs are uniquely capable of achieving. Additionally, previous studies have shown that green H_2 generated by on-site electrolyzers tends to be warm (≈320 K or above).[6] Storing this warm H_2 under cryogenic temperatures (i.e., 77 K) could lead to high refrigeration costs. For example, for cooling processes below 248 K versus 83 K, the refrigeration cost for 1 MW of cooling load increases from 18.5 $/GJ to 360 $/GJ (2017 values), respectively.[7]

Until recently, conventional MOFs for hydrogen storage required low temperatures to achieve high hydrogen uptake.[8,9] Most reported MOFs [e.g., $Zn_4O(BDC)_3$ (MOF-5, BDC^{2-} = 1,4-benzenedicarboxylate), $Cu_3(BTC)_2$ (HKUST-1, BTC^{3-} = 1,3,5-benzenetricarboxylate), and CdIF-13 (sod-Cd(benzimidazolate)$_2$)[10]] show maximum hydrogen uptake

Received: July 26, 2023

under cryogenic temperature and high-pressure conditions, whereas some emerging MOFs, such as Ni_2(*m*-dobdc) and V-btdd (*m*-dobdc^{4-} = 4,6-dioxido-1,3-benzenedicarboxylate; H_2btdd = bis(1*H*-1,2,3-triazolo[4,5-*b*],[4′,5′-*i*])dibenzo[1,4]-dioxin), exhibit record deliverable H_2 at near-ambient temperatures and high-pressure conditions (i.e., above 100 bar).[11,12] Initial findings suggested that Ni_2(*m*-dobdc) could achieve a lower levelized cost of storage ($/kWh) relative to cryogenic storage, but not compared to compressed gas storage at 350 bar without Ni_2(*m*-dobdc) being made cheaply and able to retain relatively high hydrogen uptake (i.e., below 10 $/kg and above 15 g/kg excess uptake).[5] It was also found that slower charging of the storage tank greatly reduced the cost of the associated compression and refrigeration units, further improving the promise of sorbent-based systems.

Recently, work published by researchers here has illustrated the impressive adsorptive properties of one of the simplest and lowest-cost MOF materials, aluminum formate, $Al(HCOO)_3$ (ALF). ALF adopts an ReO_3-type structure[13] and has been shown to adsorb CO_2 from dried CO_2-rich flue gas conditions with high CO_2/N_2 selectivity,[14] to selectively adsorb CO_2 from any hydrocarbon mixture, including acetylene,[15] and to provide impressive selective O_2 adsorption characteristics from O_2/N_2 mixtures above cryogenic temperatures.[16] Furthermore, ALF has very practical attributes sought for industrially utilized materials, such as withstanding pelletization, being air-stable, and being derived from cheap commodity chemicals.[14] Given the remarkable performance of ALF in these important areas as well as its alluring scalability attributes, we extended our focus to examine whether ALF could be utilized for stationary hydrogen-powered fuel cell applications.

Herein, we demonstrate that ALF displays remarkable H_2 storage performance above cryogenic temperatures (>120 K), with the most promising performance between 120 K and 160 K. We discuss the H_2 adsorption performance of ALF over the temperature range from 77 K to 296 K via gas isotherms, the crystal structure of ALF as it adsorbs D_2 gas, as resolved from in situ neutron powder diffraction, DFT calculations that support the observed performance, and technoeconomic analysis (TEA) illustrating ALF's price-competitive performance versus leading MOFs and compressed hydrogen for long-term storage. For the TEA, we show how the storage capacity of ALF, when combined with a temperature/pressure swing process, gives it clear advantages versus compressed H_2 at a fraction of the pressure.

RESULTS AND DISCUSSION

Gas Isotherm Measurements. Figure 1 displays the excess gas adsorption/desorption isotherm measurements of ALF at various temperatures plotted as a function of grams of H_2 adsorbed versus kilograms of ALF. The Supporting Information contains the same data plotted with other metrics, as well as the total adsorption plots, for comparison (Figures S1−S5). As can be seen from Figure 1, ALF shows excess adsorption of H_2 gas of ≈11 g of H_2 per kg of ALF near 120 K and ≈25 bar of pressure. As the temperature is increased, the maximum adsorption decreases, as is expected from thermodynamics. Each of the isotherms can be described as Type I isotherms, and from nonlinear Langmuir fits of the excess isotherms (Figure S6), the experimental heat of adsorption for the H_2 adsorption is 8.67 kJ/mol when treated with a single-site Langmuir model.[17] Alternative treatments

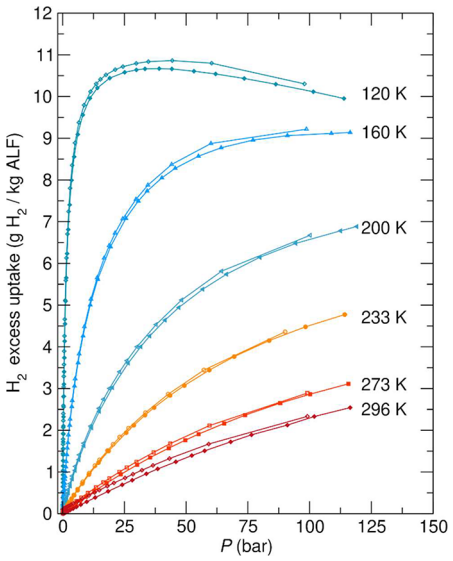

Figure 1. Excess H_2 gas adsorption/desorption isotherm measurements on ALF between 120 K and 296 K. Closed symbols = adsorption, open symbols = desorption. The same data plotted on the *y*-axis with other metrics are provided in the Supporting Information, alongside total adsorption plots and nonlinear Langmuir fits and data (Figures S1−S11, Tables S1−S4).

using a dual-site Langmuir model with lower and upper bound pore volume considerations can be found in the Supporting Information. The dual-site treatments provide similar heat of adsorption values between ≈8.5 kJ/mol and ≈9 kJ/mol as a function of loading. Given the dense, ultramicroporous nature of ALF (a material with pore sizes less than 10 Å; see previous work's supplementary materials for pore diagram)[14] when compared to many large-pore MOFs,[9,12] the adsorption values at increased pressures trend closer to values for compressed hydrogen. Figure S7 illustrates this point by showing the observed volumetric H_2 storage densities for ALF versus theoretical compressed H_2 volumetric densities (NIST WebBook)[18] of a given pressure and temperature swing process ending at 5 bar and 296 K. As such, the large initial H_2 adsorption at temperatures between 120 K and 200 K and pressures beneath 50 bar offers promising performance for H_2 storage using ALF.

As temperature is decreased below 120 K (Figures S1−S5), the inherent kinetic effects of ALF grow more pronounced, manifesting as hysteresis between adsorption and desorption curves. We have observed this phenomenon for both CO_2 and O_2 adsorption with ALF,[14,16] albeit at different temperatures, given the distinct interactions each gas has with ALF. This kinetic behavior, though curious, is not uncommon for microporous systems and has been observed in such systems as zeolite type A[19] and a non-ReO_3-type Mn(II)-formate.[20] Both materials, much like ALF, display complex sorbate−framework interactions that impact adsorption kinetics. In the case of the Mn(II)-formate material, the authors postulated that the material has "dynamic opening of the pore aperture and/or sufficient kinetic energy of the adsorbates to overcome a diffusion barrier above a critical temperature."[20] We believe that there is a similar effect in ALF and that there is likely a "critical gating temperature" which is dependent on the nature of each specific gas adsorbed into ALF.

In Situ D_2 Gas Dosing Powder Neutron Diffraction Studies. In situ D_2-dosed neutron powder diffraction

https://doi.org/10.1021/jacs.3c08037
J. Am. Chem. Soc. XXXX, XXX, XXX−XXX

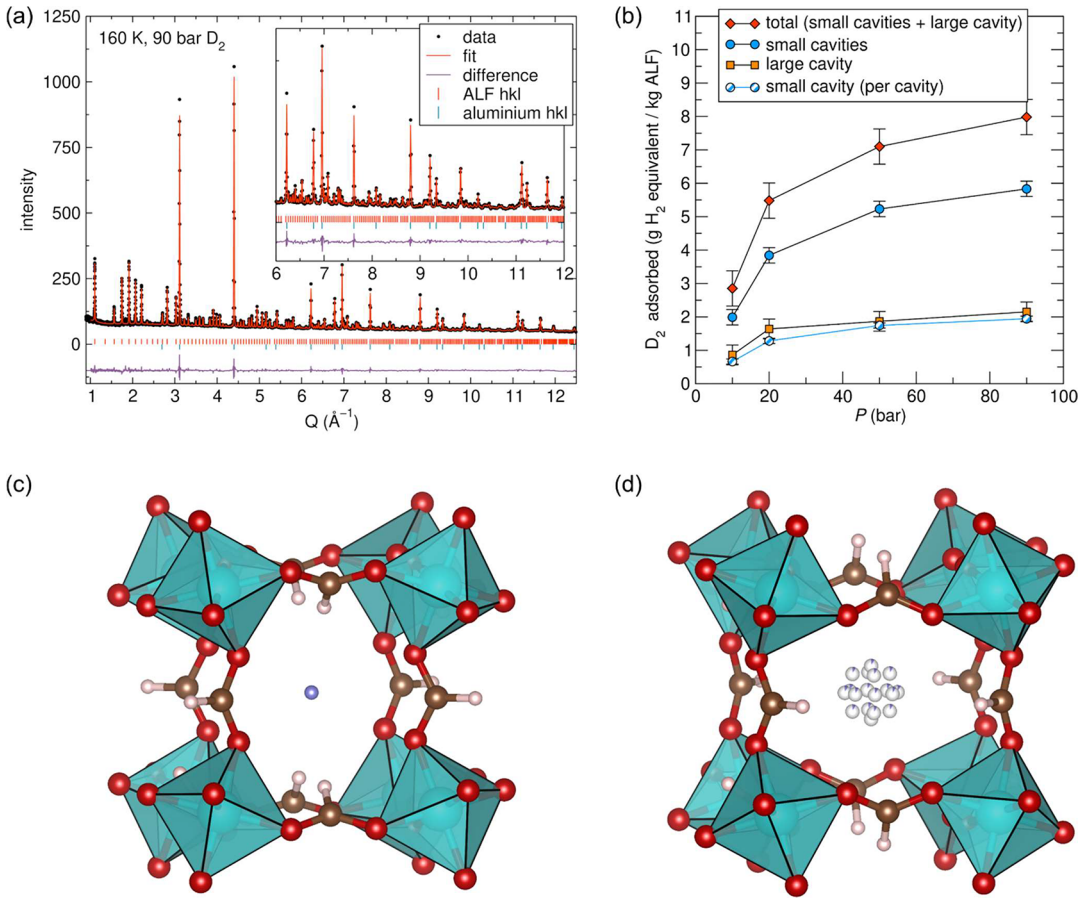

Figure 2. In situ neutron diffraction results on ALF at 160 K under D_2 pressure [ORNL, POWGEN]. (a) Representative Rietveld refinement of ALF under 90 bar of D_2. R_{wp} = 3.92%, R_p = 3.37%. Space group: $Im\bar{3}$ (No. 204). Lattice parameters, $a = b = c$ = 11.3669(1) Å. Aluminum *hkl*'s refer to solid Al high-pressure sample used for experiment, not Al metal within the sample. Refinement results can be found in the Supporting Information, Figures S12−S16, Tables S5−S9. (b) Refined values of D_2 occupancy found within ALF from the 160 K data sets for each cavity, converted into equivalent grams of H_2 per kilogram of ALF (using a molecular mass of 2 g/mol instead of 4 g/mol (D_2)) for direct comparison with Figure 1. These results are also shown in the Supporting Information (Figure S17) as a function of mmol D_2/g ALF and g D_2/kg ALF. Error bars and values denote 1σ. (c) Small cavity (SC) of ALF with D_2 super-atom at the center of the cavity. (d) Large cavity (LC) of ALF with D super-atom disordered over the surface of a sphere (radius = 0.677 Å).

experiments on ALF were conducted at the POWGEN instrument at Oak Ridge National Laboratory. Experiments were conducted at 160 K under multiple pressures of D_2 gas (0 bar, 10 bar, 20 bar, 50 bar, and 90 bar) to resolve how the structure of ALF filled and/or changed with D_2 gas. The 160 K temperature was chosen for the experiments as adsorption was known to be both fast and in high enough quantities to ensure that reliable positions of the D_2 molecules could be located within the allotted experimental time frame. Furthermore, given the fast onset of H_2 adsorption at 120 K, conducting the experiments at 160 K also allowed incremental observation of the adsorption of D_2 into the structure of the ALF to be done more precisely.

As discussed in previous work, ALF adopts an ReO_3-type structure.[13] It is akin to the perovskite structure, only instead of an *A*-site cation there is a vacancy (void space). The structure of ALF is found in the $Im\bar{3}$ space group and, as a result, has two crystallographically distinct cavities, denoted as the small cavity (SC) and large cavity (LC), which differ by how the hydrogens of the formates point toward or away from the center of each cavity, respectively. The pore volumes for the SC and LC at 300 K are 43(3) Å^3 and 79(9) Å^3, respectively.[14] For CO_2 adsorption, the SC favors CO_2 adsorption relative to the LC because the hydrogen bonding from the formate hydrogens engages in a "hand-in-glove" interaction with CO_2. This contrasts what was observed for O_2 adsorption in ALF, where hydrogen bonding in the SC is found to be less significant, with a slight preference for the LC.[16] This slight preference for the LC is observed here for D_2 adsorption as well, as we will now discuss.

Figure 2 shows select results from the in situ gas-dosed neutron powder diffraction experiments, including visualization of the D_2 positioning within the crystal structure of ALF obtained from Rietveld-derived chemical models. Figure 2a shows a representative Rietveld refinement fit of the data acquired for the highest dosed D_2 condition, 90 bar. This data set was used to confidently resolve the positions of the D_2 gas molecules adsorbed within ALF, which were then used for the lower pressure data sets. The Supporting Information shows the refinement fits obtained for the other pressures tested (0 bar, 10 bar, 20 bar, and 50 bar). Specific to the refinements, the gas molecules were modeled as "super-atoms", given that D_2 is a quantum object and the molecular dumbbell is orientationally averaged to produce a more spherical scattering center, as is typically observed in the literature.[12,21−24] Practically, this means that an appropriate Rietveld refinement will use a single

https://doi.org/10.1021/jacs.3c08037
J. Am. Chem. Soc. XXXX, XXX, XXX−XXX

D atom, instead of a D_2 molecule, to describe a D_2 molecular position. In the refinements, each D super-atom was allowed a maximum occupancy of 2 to account for the modeling of a D_2 molecule.

Figure 2b shows the refined amounts of D_2 adsorbed in ALF as derived from the Rietveld refinements over the range of pressures studied. The amounts graphed are the total amount adsorbed at each pressure, as well as the amount for each cavity. The occupancies in Figure 2b have been converted to grams of H_2 per kilogram of ALF, for direct comparison with the isotherm data in Figure 1. The metrics in mmol of D_2 per g of ALF, and g of D_2 per kg of ALF, are also found in the Supporting Information (Figure S17). Tables S5−S9 in the Supporting Information show the crystallographic occupancies from the refinements prior to conversion. As can be appreciated, the power of the in situ gas dosing neutron diffraction experiments is that the Rietveld refinements with such data provide real-space context as to how gases interact with an adsorbent.[25] In this instance, we found that, at all D_2 pressures tested, and given that ALF has two distinct cavities, the SC and LC, both cavities adsorbed D_2 gas in nearly equal amounts after equilibration when normalized for multiplicity. This is shown in Figure 2b when comparing the D_2 occupancy of the LC versus the D_2 occupancy found in just one SC (there are 3 times as many SCs versus LCs within ALF, given the $Im\bar{3}$ symmetry).

Though D_2 is adsorbed into each of the cavities in nearly equal proportions, how the D_2 molecules fill within the two cavities is distinct. Figure 2c,d illustrates how the D super-atoms are found within the SCs and LCs, respectively, as resolved from the Rietveld refinement with the data at 160 K and 90 bar D_2 pressure. The SC D super-atom was found to be best modeled with one position at the special position [0, 1/2, 0], which is the center of the SC. Attempts were made to move the super-atom off this special position within the SC, which in principle could describe any preferential positioning within the cavity. However, no position away from the [0, 1/2, 0] position was found to statistically improve the fit or provide any other convincing indications of localization. Instead, the most stable and statistically consistent result was modeled with a super-atom at the center of the cavity with a large isotropic Debye−Waller factor, B_{eq} (refined and stable B_{eq} value of ≈14 Å^2). This result implies that the D_2 inside of the SC is, on average, localized at the center of the cavity, albeit likely somewhat dynamic under these conditions.

This result contrasts with what was found to be the case for the LC, where if the D super-atoms were modeled at the center of the LC, they had a refined B_{eq} of ≈14.2 Å^2, similar to that of the SC D super-atom. However, if they were displaced from the special position so as to populate the surface of the sphere inside of the LC, the B_{eq} values of the D super-atoms were reduced and stabilized by an order of magnitude to ≈1.7 Å^2. This spherical surface modeling is shown in Figure 2d. This indicates that there is preferential adsorption of the D_2 gas toward the surfaces of the LC walls/ligands, as opposed to occupying the center of the cavity. The distinction in the localization of D_2 within the two cavities can be rationalized given that there is likely vibrational movement of the formates/formate hydrogens at these temperatures that would constantly perturb the location of the D_2 molecules when at the center of the SC. Given that the LC has no such formate hydrogens that point inward, the D_2 molecules could be expected to be comparatively undisturbed, as they associate with the formate ligands' O−C−O backbone through weak electrostatic and other dispersion forces. This model is further supported by a DFT-derived heatmap for H_2 positional energy inside the cavities of ALF. The heatmap suggests the existence of a shallow energy landscape for H_2 toward the walls of the LC, contrasting with a clear localized low-energy landscape for H_2 positioned at the center of the SC (Figure S18). There is also excellent agreement between the total hydrogen capacity of the pores and that expected from the 160 K adsorption isotherm.

Furthermore, in agreement with our diffraction and isotherm results, the DFT-calculated H_2 heats of adsorption for each of the cavities are found to be 11.66 kJ/mol and 12.54 kJ/mol for the SC and LC, respectively (details in Supporting Information). These similarly valued heats of adsorption for the two cavities align well with what was seen from diffraction, which suggests that H_2 fills both cavities with comparable amounts, with a slight preference for the LC. The DFT-calculated heat of adsorption values are also close to the isotherm-derived heat of adsorption of 8.67 kJ/mol (fitting from nonlinear Langmuir fits to the adsorption data 120 K to 297 K, Figure S6). It is understood from the literature that the optimal heat of adsorption for hydrogen storage materials at ambient conditions should be between 15 kJ/mol and 25 kJ/mol.[12]

Technoeconomic Analysis (TEA) of Stationary Long-Duration H_2 Storage Using ALF. Materials proposed for on-board H_2 use,[26−29] including V-btdd[12] and Ni_2(*m*-dobdc),[11] are judged most significantly by their high H_2 storage densities as close to room temperature as possible. This contrasts with the requirements of long-duration H_2 storage materials, where H_2 storage density is not the most important factor, given that space is not limited as it would be in a vehicle. Instead, materials for long-duration H_2 storage are judged by their general performance (adsorption per T and P), scalability, and cost. ALF distinguishes itself in this regard from most MOF materials proposed for long-duration H_2 storage by being derived from low-cost commodity chemicals and still achieving high H_2 uptakes at low working pressures and non-cryogenic temperatures. We evaluate the impact of these characteristics on the cost for an on-site, large-scale (10 MW), and long-duration (96 h) stationary H_2 storage application to meet backup power needs (8 cycles per year). We note that, while the reported cycle lives for many MOFs are from 1000 cycles to 5000 cycles,[30,31] the effects of replacement and stability should be evaluated for future studies requiring more operation cycles. Low-pressure operation is compelling, as a storage pressure between 10 bar and 25 bar is all that is needed for serving the pressure requirements of stationary fuel cells operating at 2 bar to 10 bar.[32] Beyond economic considerations, operating storage systems at low pressures also greatly reduces the safety concerns and system complexity when dispensing H_2, providing lower system costs and fostering general public acceptance of the technology.

With regard to material costs, at high manufacturing rates, it has been suggested that emerging MOFs that are manufactured using abundant metals, such as nickel or zinc, can achieve a material cost of 10 $/kg of MOF.[33] Lowering the MOF manufacture cost to the level of ≈2 $/kg, which is expected with ALF given that it is made from the abundant commodity chemical reagents aluminum hydroxide and formic acid (priced at 0.3 $/kg to 0.5 $/kg and 0.5 $/kg to 0.9 $/kg wholesale costs, respectively, Supporting Information), provides a cost reduction with substantial promise. ALF avoids the use of

https://doi.org/10.1021/jacs.3c08037
J. Am. Chem. Soc. XXXX, XXX, XXX−XXX

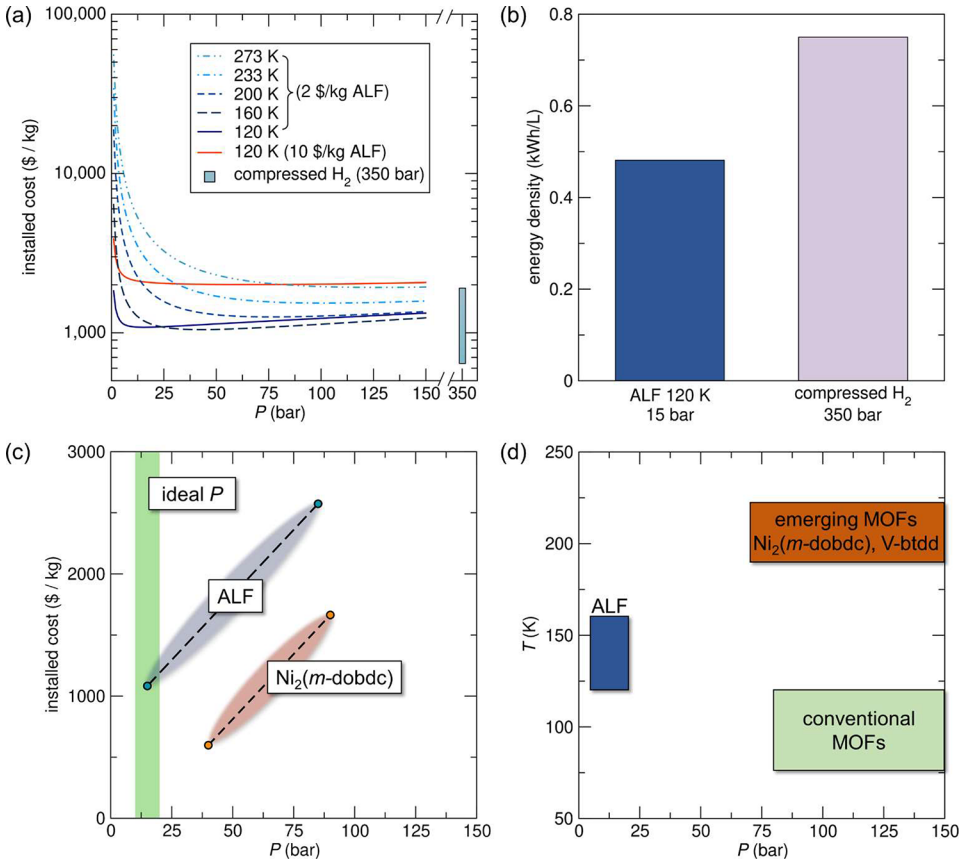

Figure 3. Technoeconomic analysis (TEA) and system-level performance of ALF vs compressed gas and other MOFs. (a) Modeled installed capital cost for ALF at different temperatures and pressures when the charging rate is half of the discharge rate. The red line shows the installed cost if ALF was priced at 10 $/kg. Compressed gas installed costs at 350 bar are shown by the light blue bar. (b) Comparison of system-level energy density of ALF with compressed hydrogen storage under 350 bar (293 K), calculated based on the amount of hydrogen stored in a tank and the tank's outer volume. (c) Comparison of ALF with a top-performing contemporary MOF (Ni_2(*m*-dobdc)) under optimum cost and pressures versus under different manufacturing costs and operating conditions [low-cost value, 2 $/kg with moderate charging (charge = 0.5 times discharge) and high-cost value, 10 $/kg with fast charging (charge = 4 times faster than the discharge) for both MOFs]. The green area denotes the ideal delivery pressure range (10 bar to 20 bar) for stationary applications when coupled with fuel cells. Dashed lines between the two data points for ALF and Ni_2(*m*-dobdc) are used for an easier comparison between the ranges. The shaded region behind the line denotes that values between the two ranges can vary. (d) Schematic diagram depicting the optimum range of temperature and pressure conditions for different types of MOFs.

comparatively complex organic reagents such as 2,5-dihydroxyterephthalic acid or metal salts such as nickel nitrate (priced at 2 $/kg to 20 $/kg and 3 $/kg to 15 $/kg, respectively, Supporting Information). Assuming a conservative material cost of 2 $/kg and based on the H_2 excess uptake with ALF (Figure 1) and its other fundamental properties (density, specific heat, etc.), we find that a minimum installed cost is achieved at a working pressure near 15 bar (Figure 3a). At this pressure and under moderate cooling (120 K), the modeled ALF (with packing density of 1429 kg/m^3) achieves approximately two-thirds of the system-level energy density of 350 bar compressed gas storage at ambient conditions (Figure 3b). This represents a ≈95% pressure reduction for comparable performance when using ALF. Furthermore, we again mention that ALF withstands pelletization and ball-milling,[14] making it promising to achieve high packing densities during deployment, which contributes to high system-level energy density.

If such low material costs can be achieved, ALF offers an installed cost that is lower than those of 350 bar compressed gas systems, despite its cooling requirement (Figure 3a). This is true even at a working temperature of 273 K; however, more pressure is required for ALF to achieve costs that are comparable with those of 350 bar compressed gas systems. A low material cost, such as ALF, would also put the capital cost of a MOF on par with other system components, such as compressors and refrigerators (Supporting Information, Figure S19). We compare ALF to an emerging leader for H_2 storage, Ni_2(*m*-dobdc), to illustrate each material's optimal operation range based on their cost performance across 120 K to 293 K and 0 bar to 170 bar (Figure 3c). The findings are remarkable, as both ALF and Ni_2(*m*-dobdc) could achieve a lower installed cost than 350 bar compressed gas systems. To our knowledge, this is the first study where sorbent-based hydrogen storage outperforms cryogenic and compressed gas technologies in a hydrogen storage application.

Lastly, the unique adsorption attributes of ALF compared to contemporary MOFs provide new opportunities for future applications for H_2 storage (Figure 3d). ALF's optimum conditions use moderate cooling and low pressures to achieve high storage, potentially making ALF suitable for applications where a precooled hydrogen stream requires storage, as may be the case for the capture of cryogenic boil-off gas.[34]

https://doi.org/10.1021/jacs.3c08037
J. Am. Chem. Soc. XXXX, XXX, XXX−XXX

CONCLUSION

Herein, we have shown that aluminum formate (ALF), which adopts the ReO_3-type structure, adsorbs H_2 at non-cryogenic temperatures with an experimental heat of adsorption of ≈8.6 kJ/mol. From the in situ neutron diffraction analysis of D_2-dosed ALF, we show how both of ALF's cavities fill at comparable levels. Specifically, the large cavity of ALF has more localized D_2 molecules near the walls of the framework, while in the small cavity D_2 molecules are located near the center. The adsorption isotherms show that the optimal performance of ALF is found at relatively low pressures (around 25 bar), where the total uptake is near 12 g of H_2/kg of ALF at 120 K. Most importantly, ALF's H_2 adsorption performance makes it unique compared to other reported MOFs for low-pressure applications at intermediate temperatures.

From TEA, we have shown that ALF is the only MOF to date to achieve cost parity with 350 bar compressed gas storage at a working pressure within the ideal operation range for safe storage systems serving fuel cells. This is achieved at non-cryogenic temperatures, with the best cost performance found between 120 K and 160 K. Given its lower pressure adsorption performance, ALF also shows promise in emerging H_2 storage/capture areas of interest, such as H_2 boil-off capture. These results are impressive alone but are further amplified by the practical attributes of ALF for industrially relevant processes. First, ALF is pelletizable, as demonstrated previously,[14] contrasting many large void space MOFs that often amorphize upon pelletization.[35] Second, ALF is chemically robust, withstanding weeks at ambient air conditions without major degradation.[14] Lastly, as ALF is made from cheap and ubiquitous commodity chemicals, it faces fewer challenges in scalability compared to most other MOFs (note our previous demonstration of kilogram-scale synthesis of ALF using laboratory methods[14]). Such characteristics are key for unlocking opportunities for sorbent-based hydrogen storage, as are the proper identification of market applications with sorbent behavior and ideal operating conditions. As cooling adds refrigeration costs, ALF will benefit from applications where low pressure and cool or near-ambient hydrogen are available and storage is required.

ASSOCIATED CONTENT

Supporting Information

The Supporting Information is available free of charge at https://pubs.acs.org/doi/10.1021/jacs.3c08037.

Experimental details and supporting figures and tables (PDF)

Accession Codes

CCDC 2264160 contains the supplementary crystallographic data for this paper. These data can be obtained free of charge via www.ccdc.cam.ac.uk/data_request/cif, or by emailing data_request@ccdc.cam.ac.uk, or by contacting The Cambridge Crystallographic Data Centre, 12 Union Road, Cambridge CB2 1EZ, UK; fax: +44 1223 336033.

AUTHOR INFORMATION

Corresponding Authors

Hayden A. Evans − *Center for Neutron Research, National Institute of Standards and Technology, Gaithersburg, Maryland 20899, United States;* orcid.org/0000-0002-1331-4274; Email: hayden.evans@nist.gov

Taner Yildirim − *Center for Neutron Research, National Institute of Standards and Technology, Gaithersburg, Maryland 20899, United States;* Email: taner.yildirim@nist.gov

Craig M. Brown − *Center for Neutron Research, National Institute of Standards and Technology, Gaithersburg, Maryland 20899, United States;* orcid.org/0000-0002-9637-9355; Email: craig.brown@nist.gov

Authors

Peng Peng − *Energy Analysis and Environmental Impacts Division, Lawrence Berkeley National Laboratory, Berkeley, California 94720, United States;* orcid.org/0000-0001-6554-2247

Yongqiang Cheng − *Neutron Scattering Division, Oak Ridge National Laboratory, Oak Ridge, Tennessee 37830, United States;* orcid.org/0000-0002-3263-4812

Zeyu Deng − *Department of Materials Science and Engineering, National University of Singapore, 117575, Singapore;* orcid.org/0000-0003-0109-9367

Qiang Zhang − *Neutron Scattering Division, Oak Ridge National Laboratory, Oak Ridge, Tennessee 37830, United States;* orcid.org/0000-0003-0389-7039

Dinesh Mullangi − *Department of Materials Science and Engineering, National University of Singapore, 117575, Singapore;* orcid.org/0000-0003-4012-0587

Dan Zhao − *Department of Chemical and Biomolecular Engineering, National University of Singapore, 117575, Singapore;* orcid.org/0000-0002-4427-2150

Pieremanuele Canepa − *Department of Materials Science and Engineering, National University of Singapore, 117575, Singapore;* orcid.org/0000-0002-5168-9253

Hanna M. Breunig − *Energy Analysis and Environmental Impacts Division, Lawrence Berkeley National Laboratory, Berkeley, California 94720, United States;* orcid.org/0000-0002-4727-424X

Anthony K. Cheetham − *Department of Materials Science and Engineering, National University of Singapore, 117575, Singapore; Materials Research Laboratory, University of California, Santa Barbara, California 93106, United States;* orcid.org/0000-0003-1518-4845

Complete contact information is available at: https://pubs.acs.org/10.1021/jacs.3c08037

Notes

Certain commercial equipment, instruments, or materials are identified in this document. Such identification does not imply recommendation or endorsement by the National Institute of Standards and Technology, nor does it imply that the products identified are necessarily the best available for the purpose.

The authors declare the following competing financial interest(s): A patent has been filed protecting certain information disclosed within this manuscript.

ACKNOWLEDGMENTS

We acknowledge NIST for partial funding for this work. The authors gratefully acknowledge partial support from the Hydrogen Materials—Advanced Research Consortium (HyMARC) established as part of the Energy Materials Network under the U.S. DOE Office of Energy Efficiency and Renewable Energy (EERE), Hydrogen and Fuel Cell Technologies Office, under contract number DE-AC02-05CH11231 with Lawrence Berkeley National Laboratory

(H.M.B., P.P.). A portion of this research used resources at the Spallation Neutron Source [POWGEN], a DOE Office of Science User Facility operated by the Oak Ridge National Laboratory. Y.C. and Q.Z. thank Mark Loguillo and Matt Rucker for their assistance with sample environment setup. We thank the Singapore MOE-Academic Research Fund (R-284-000-193-114) (D.M., A.K.C.), the National University of Singapore Green Energy Programme for partial funding under the project code R-284-000-185-731 (A.K.C., D.Z., P.C.), the Agency for Science, Technology and Research (U2102d2004) (D.Z.), and the Ras al Khaimah Centre for Advanced Materials (A.K.C.). Z.D. acknowledges support from a Lee Kuan Yew Postdoctoral Fellowship (22-5930-A0001). We thank Ryan Klein (NREL) for fruitful discussion.

REFERENCES

(1) Goldsmith, J.; Wong-Foy, A. G.; Cafarella, M. J.; Siegel, D. J. Theoretical Limits of Hydrogen Storage in Metal−Organic Frameworks: Opportunities and Trade-Offs. *Chem. Mater.* **2013**, *25* (16), 3373−3382.

(2) Hunter, C. A.; Penev, M. M.; Reznicek, E. P.; Eichman, J.; Rustagi, N.; Baldwin, S. F. Techno-Economic Analysis of Long-Duration Energy Storage and Flexible Power Generation Technologies to Support High-Variable Renewable Energy Grids. *Joule* **2021**, *5* (8), 2077−2101.

(3) Ma, Z.; Eichman, J.; Kurtz, J. Fuel Cell Backup Power System for Grid Service and Microgrid in Telecommunication Applications. *J. Energy Resour. Technol.* **2019**, *141* (6), 062002.

(4) Sathe, R. Y.; Dhilip Kumar, T. J.; Ahuja, R. Furtherance of the Material-Based Hydrogen Storage Based on Theory and Experiments. *Int. J. Hydrog. Energy* **2023**, *48* (34), 12767−12795.

(5) Peng, P.; Anastasopoulou, A.; Brooks, K.; Furukawa, H.; Bowden, M. E.; Long, J. R.; Autrey, T.; Breunig, H. Cost and Potential of Metal−Organic Frameworks for Hydrogen Back-up Power Supply. *Nat. Energy* **2022**, *7* (5), 448−458.

(6) Haug, P.; Kreitz, B.; Koj, M.; Turek, T. Process Modelling of an Alkaline Water Electrolyzer. *Int. J. Hydrog. Energy* **2017**, *42* (24), 15689−15707.

(7) Luyben, W. L. Estimating Refrigeration Costs at Cryogenic Temperatures. *Comput. Chem. Eng.* **2017**, *103*, 144−150.

(8) Gómez-Gualdrón, D. A.; Colón, Y. J.; Zhang, X.; Wang, T. C.; Chen, Y.-S.; Hupp, J. T.; Yildirim, T.; Farha, O. K.; Zhang, J.; Snurr, R. Q. Evaluating Topologically Diverse Metal−Organic Frameworks for Cryo-Adsorbed Hydrogen Storage. *Energy Environ. Sci.* **2016**, *9* (10), 3279−3289.

(9) Bobbitt, N. S.; Chen, J.; Snurr, R. Q. High-Throughput Screening of Metal−Organic Frameworks for Hydrogen Storage at Cryogenic Temperature. *J. Phys. Chem. C* **2016**, *120* (48), 27328−27341.

(10) Halder, A.; Klein, R. A.; Shulda, S.; McCarver, G. A.; Parilla, P. A.; Furukawa, H.; Brown, C. M.; McGuirk, C. M. Multivariate Flexible Framework with High Usable Hydrogen Capacity in a Reduced Pressure Swing Process. *J. Am. Chem. Soc.* **2023**, *145* (14), 8033−8042.

(11) Kapelewski, M. T.; Runčevski, T.; Tarver, J. D.; Jiang, H. Z. H.; Hurst, K. E.; Parilla, P. A.; Ayala, A.; Gennett, T.; FitzGerald, S. A.; Brown, C. M.; Long, J. R. Record High Hydrogen Storage Capacity in the Metal−Organic Framework Ni_2(m-Dobdc) at near-Ambient Temperatures. *Chem. Mater.* **2018**, *30* (22), 8179−8189.

(12) Jaramillo, D. E.; Jiang, H. Z. H.; Evans, H. A.; Chakraborty, R.; Furukawa, H.; Brown, C. M.; Head-Gordon, M.; Long, J. R. Ambient-Temperature Hydrogen Storage via Vanadium(II)-Dihydrogen Complexation in a Metal−Organic Framework. *J. Am. Chem. Soc.* **2021**, *143* (16), 6248−6256.

(13) Evans, H. A.; Wu, Y.; Seshadri, R.; Cheetham, A. K. Perovskite-Related ReO_3-Type Structures. *Nat. Rev. Mater.* **2020**, *5* (3), 196−213.

(14) Evans, H. A.; Mullangi, D.; Deng, Z.; Wang, Y.; Peh, S. B.; Wei, F.; Wang, J.; Brown, C. M.; Zhao, D.; Canepa, P.; Cheetham, A. K. Aluminum Formate, $Al(HCOO)_3$: An Earth-Abundant, Scalable, and Highly Selective Material for CO_2 Capture. *Sci. Adv.* **2022**, *8* (44), No. eade1473.

(15) Zhang, Z.; Deng, Z.; Evans, H. A.; Mullangi, D.; Kang, C.; Peh, S. B.; Wang, Y.; Brown, C. M.; Wang, J.; Canepa, P.; Cheetham, A. K.; Zhao, D. Exclusive Recognition of CO_2 from Hydrocarbons by Aluminum Formate with Hydrogen-Confined Pore Cavities. *J. Am. Chem. Soc.* **2023**, *145* (21), 11643−11649.

(16) Mullangi, D.; Evans, H. A.; Yildirim, T.; Wang, Y.; Deng, Z.; Zhang, Z.; Mai, T. T.; Wei, F.; Wang, J.; Hight Walker, A. R.; Brown, C. M.; Zhao, D.; Canepa, P.; Cheetham, A. K. Noncryogenic Air Separation Using Aluminum Formate $Al(HCOO)_3$ (ALF). *J. Am. Chem. Soc.* **2023**, *145* (17), 9850−9856.

(17) Swenson, H.; Stadie, N. P. Langmuir's Theory of Adsorption: A Centennial Review. *Langmuir* **2019**, *35* (16), 5409−5426.

(18) Linstrom, P. J.; Mallard, W. G. *NIST Chemistry WebBook*, NIST Standard Reference Database Number 69; National Institute of Standards and Technology, 2017. DOI: 10.1021/je000236i.

(19) Breck, D. W.; Eversole, W. G.; Milton, R. M.; Reed, T. B.; Thomas, T. L. Crystalline Zeolites. I. The Properties of a New Synthetic Zeolite, Type A. *J. Am. Chem. Soc.* **1956**, *78* (23), 5963−5972.

(20) Kim, H.; Samsonenko, D. G.; Yoon, M.; Yoon, J. W.; Hwang, Y. K.; Chang, J.-S.; Kim, K. Temperature-Triggered Gate Opening for Gas Adsorption in Microporous Manganese Formate. *Chem. Commun.* **2008**, *39*, 4697−4699.

(21) Brown, C. M.; Liu, Y.; Yildirim, T.; Peterson, V. K.; Kepert, C. J. Hydrogen Adsorption in HKUST-1: A Combined Inelastic Neutron Scattering and First-Principles Study. *J. Energy Resour. Technol.* **2009**, *20*, 204025.

(22) Pollock, R. A.; Her, J.-H.; Brown, C. M.; Liu, Y.; Dailly, A. Kinetic Trapping of D_2 in MIL-53(Al) Observed Using Neutron Scattering. *J. Phys. Chem. C* **2014**, *118* (31), 18197−18206.

(23) Wu, H.; Zhou, W.; Yildirim, T. Hydrogen Storage in a Prototypical Zeolitic Imidazolate Framework-8. *J. Am. Chem. Soc.* **2007**, *129* (17), 5314−5315.

(24) Barnett, B. R.; Evans, H. A.; Su, G. M.; Jiang, H. Z. H.; Chakraborty, R.; Banyeretse, D.; Hartman, T. J.; Martinez, M. B.; Trump, B. A.; Tarver, J. D.; Dods, M. N.; Funke, L. M.; Börgel, J.; Reimer, J. A.; Drisdell, W. S.; Hurst, K. E.; Gennett, T.; FitzGerald, S. A.; Brown, C. M.; Head-Gordon, M.; Long, J. R. Observation of an Intermediate to H_2 Binding in a Metal−Organic Framework. *J. Am. Chem. Soc.* **2021**, *143* (36), 14884−14894.

(25) Klein, R. A.; Evans, H. A.; Trump, B. A.; Udovic, T. J.; Brown, C. M. 10.02 - Neutron Scattering Studies of Materials for Hydrogen Storage. In *Comprehensive Inorganic Chemistry III*, 3rd ed.; Reedijk, J., Poeppelmeier, K. R., Eds.; Elsevier: Oxford, 2023; pp 3−50. DOI: 10.1016/B978-0-12-823144-9.00028-5.

(26) Sofianos, M. V.; Sheppard, D. A.; Ianni, E.; Humphries, T. D.; Rowles, M. R.; Liu, S.; Buckley, C. E. Novel Synthesis of Porous Aluminium and Its Application in Hydrogen Storage. *J. Alloys Compd.* **2017**, *702*, 309−317.

(27) Sathe, R. Y.; Dhilip Kumar, T. J. Electronic Structure Calculations of Reversible Hydrogen Storage in Nanoporous Ti Cluster Frameworks. *ACS Appl. Nano Mater.* **2020**, *3* (6), 5575−5582.

(28) Simanullang, M.; Prost, L. Nanomaterials for On-Board Solid-State Hydrogen Storage Applications. *Int. J. Hydrog. Energy* **2022**, *47* (69), 29808−29846.

(29) Liang, L.; Yang, Q.; Zhao, S.; Wang, L.; Liang, F. Excellent Catalytic Effect of LaNi5 on Hydrogen Storage Properties for Aluminium Hydride at Mild Temperature. *Int. J. Hydrog.* **2021**, *46* (78), 38733−38740.

(30) Anastasopoulou, A.; Furukawa, H.; Barnett, B. R.; Jiang, H. Z. H.; Long, J. R.; Breunig, H. M. Technoeconomic Analysis of Metal−Organic Frameworks for Bulk Hydrogen Transportation. *Energy Environ. Sci.* **2021**, *14* (3), 1083−1094.

https://doi.org/10.1021/jacs.3c08037
J. Am. Chem. Soc. XXXX, XXX, XXX−XXX

(31) Lenzen, D.; Zhao, J.; Ernst, S.-J.; Wahiduzzaman, M.; Ken Inge, A.; Fröhlich, D.; Xu, H.; Bart, H.-J.; Janiak, C.; Henninger, S.; Maurin, G.; Zou, X.; Stock, N. A Metal−Organic Framework for Efficient Water-Based Ultra-Low-Temperature-Driven Cooling. *Nat. Commun.* **2019**, *10* (1), 3025.
(32) Wong, C. Y.; Wong, W. Y.; Ramya, K.; Khalid, M.; Loh, K. S.; Daud, W. R. W.; Lim, K. L.; Walvekar, R.; Kadhum, A. A. H. Additives in Proton Exchange Membranes for Low- and High-Temperature Fuel Cell Applications: A Review. *Int. J. Hydrog. Energy* **2019**, *44* (12), 6116−6135.
(33) DeSantis, D.; Mason, J. A.; James, B. D.; Houchins, C.; Long, J. R.; Veenstra, M. Techno-Economic Analysis of Metal−Organic Frameworks for Hydrogen and Natural Gas Storage. *Energy Fuels* **2017**, *31* (2), 2024−2032.
(34) Petitpas, G. *Boil-off Losses along LH2 Pathway*; LLNL-TR-750685; Lawrence Livermore National Laboratory, Livermore, CA, 2018. DOI: 10.2172/1466121.
(35) Tan, J. C.; Cheetham, A. K. Mechanical Properties of Hybrid Inorganic−Organic Framework Materials: Establishing Fundamental Structure−Property Relationships. *Chem. Soc. Rev.* **2011**, *40* (2), 1059−1080.

https://doi.org/10.1021/jacs.3c08037
J. Am. Chem. Soc. XXXX, XXX, XXX−XXX